Simple Law for Third-Body Friction

Fei Deng,[1,†] Georgios Tsekenis,[1,†] and Shmuel M. Rubinstein[1,2,*]
[1]Harvard John A. Paulson School of Engineering and Applied Sciences, Harvard University, Cambridge, Massachusetts 02138, USA
[2]Kavli Institute for Bionano Science and Technology, Harvard University, Cambridge, Massachusetts 02138, USA

(Received 24 August 2018; published 5 April 2019)

A key difficulty to understanding friction is that many physical mechanisms contribute simultaneously. Here we investigate third-body frictional dynamics in a model experimental system that eliminates first-body interaction, wear, and fracture, and concentrates on the elastic interaction between sliding blocks and third bodies. We simultaneously visualize the particle motion and measure the global shear force. By systematically increasing the number of foreign particles, we find that the frictional dissipation depends only on the size ratio between surface asperities and the loose particles, irrespective of the particle's size or the surface's roughness. When the particles are comparable in size to the surface features, friction increases linearly with the number of particles. For particles smaller than the surface features, friction grows sublinearly with the number of particles. Our findings suggest that matching the size of surface features to the size of potential contaminants may be a good strategy for reliable lubrication.

DOI: 10.1103/PhysRevLett.122.135503

Introduction.—The dynamical resistance of two contacting bodies to relative motion, or friction, is commonly considered [1–7] to depend on their material properties. For practical purposes, two nominally flat sliding solids are usually considered, and friction is characterized by a single parameter: the coefficient of friction [8]. Today, it is accepted that friction is a dynamic process [9,10] and that the friction coefficient may depend on many factors, such as loading geometry [11–13], sliding rate [5,14,15], and sliding history [16–20]. However, these effects typically modify friction relative to its material-determined base state. More remarkable is the impact of third bodies, or phases, frequently found to infect sliding interfaces (whether purposefully or not), which can completely alter the frictional dynamics [21–24]. Materials rubbed repetitively wear when films or loose particles get trapped within the interface and agglomerate into load-carrying third bodies. In a tribological system, a fluid body (or phase) introduced into the interface can alter the dynamics [25–31]. Third bodies, gouge, and wear play an especially critical role in geological physics as the frictional dynamics between rocks of disparate scales, from granular media to tectonic plates [32], are affected by gouge-filled damage zones of various granular phases that often dominate the sliding dynamics and stability of shear zones and tectonic faults [33–39]. Indeed, granular flow and deformation of granular systems at high densities have been studied extensively, revealing a complex rheological response under shear [40–42] and robust constitutive laws for granular flow [43–45]. In sliding systems with a small number of third-body particles, experimental and numerical studies have produced a wealth of empirical knowledge [46–50]. Experimentally, however, it is difficult to isolate the role of third-body friction from other effects, such as wear.

In this work, we experimentally isolate the effect of third-body particles on macroscopic solid friction. We perform a systematic study of the frictional resistance between two rough surfaces as discrete particles are introduced into the interface. We focus on the effects of the particles by keeping the sliding surfaces at a fixed gap—not a fixed perpendicular load. We show that even one particle can qualitatively alter the sliding dynamics. As expected, frictional dissipation increases as more particles are added to the interface. However, the rate of increase of the dissipation depends on the ratio between the size of the particles and the typical feature size of the interface; if the size ratio is one or larger, frictional force grows linearly with particle number. If the size ratio is less than one, the increase in frictional force with particle number N grows as N^{β}, where $\beta < 1$.

Results.—The major challenge in studying third-body-induced friction is to isolate the third-body friction effects. To this end, we developed an experimental system that probes the role of small, third-body particulates in sliding friction while suppressing other effects, as shown in Fig. 1(a). Our sliding surfaces are composed of two ring-shaped samples cast out of polydimethylsiloxane (PDMS). The rings are 3.5 mm wide with an outer diameter of 22 mm. The molds are 3D printed and designed to have two qualitatively different surface patterns: (i) disordered with randomly distributed single-cosine-shaped asperities, and (ii) ordered with a two-dimensional grid of perpendicular sinusoids. We cast the samples out of the molds shown in

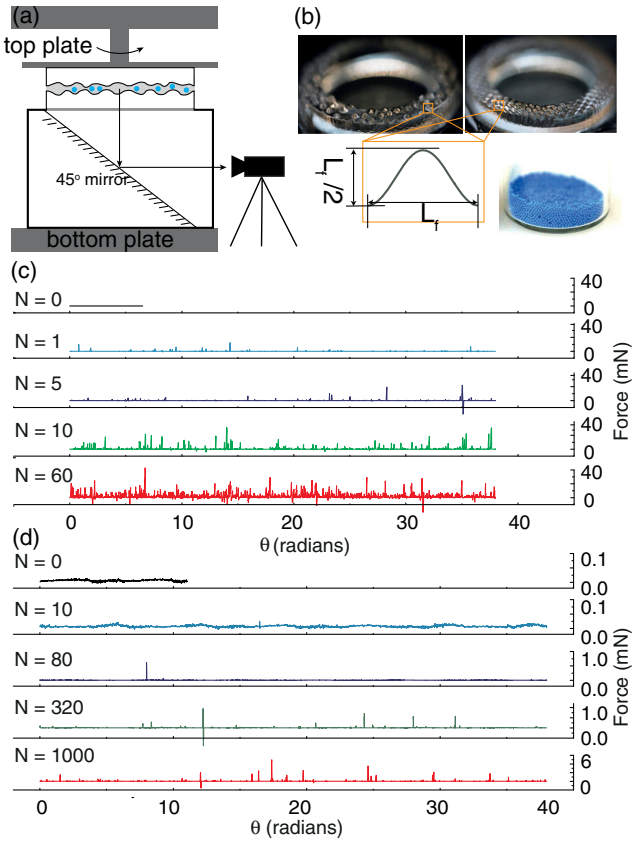

FIG. 1. Experimental setup and raw data. (a) Schematic of experimental setup. (b) The PDMS rings with disordered (left) and ordered (right) surfaces with cosine asperities, as well as two sizes of polyethylene particles. (c) Shear force time series for $\Delta = 1.45$ and (d) for $\Delta = 0.5$ on disordered surfaces. The initial force times series ($N = 0$) contain oil and no particles. The number of added particles increases downward within each panel.

Fig. 1(b). We define roughness of all surfaces to be the characteristic asperity size L_f; each asperity has the shape of a cosine bump with an aspect ratio of width to height of 2. In this study, we used patterns with L_f ranging from 250–625 μm. The particles used are made of polyethylene and are much harder than the PDMS rings. (See the Supplemental Material [51] for details.)

Two elastic PDMS rings with identical surface patterns are coupled to the bottom and top plates of a commercial rheometer (see the Supplemental Material [51]), a device used to measure how liquids or liquid-solid mixtures respond to applied forces. The two rubber rings sit parallel and concentric to one another with their rough sides facing each other at a vertical gap that allows them to freely rotate without contact. However, the rough surfaces are close enough that the minimum vertical distance between the two surfaces over an entire rotation is less than 10 μm. For our experiments, the minimum intersurface distance varies by 5 ± 2.5 μm. (Details on how we achieved the small gap are included in the Supplemental Material [51].) At the beginning of every experiment, we check that the system shows no measurable shear force after the gap is filled with low viscosity silicone oil, as shown for $N = 0$ in Fig. 1(c).

The space between the rough surfaces is filled with silicone oil matching the refractive index of the PDMS rings but not that of the polyethylene particles. This allows us to simultaneously visualize the interfacial particle dynamics while measuring the global shear force. Silicone oil has a 3% lower density than the polyethylene particles [Fig. 1(b)]; thus, the particles preferentially sink into the valleys of the bottom surface. However, the density difference is low enough for low-velocity flows to lift and carry the particles up and around, resulting in stochastic dynamics. The top plate is rotated at a set rate while the torque (shear force) is measured as a function of the rotation angle (which, for constant rotational velocity, is proportional to time). The load is also measured. Particles are introduced incrementally into the interface at increasing numbers, N. Several particles diameters, D_b, were tested, ranging from 98–550 μm. The characteristic size ratio of the system is defined as $\Delta = D_b/L_f$. A constant rotation speed of 0.01 rad/s was used in all tests. This relatively slow rate reduces the viscous forces induced by the shearing of the silicone oil, thus allowing resolution of smaller discrete frictional force peaks generated through the disturbance caused by a single particle.

The particle-free interface purposefully exhibits exceptionally low resistance. Indeed, when the interface is filled only with silicone oil ($N = 0$), the shear force measured by the rheometer never exceeds 0.04 mN. However, the addition of even a single particle ($N = 1$) dramatically modifies the sliding dynamics. The total frictional dissipation increases, and discrete random shear force peaks as high as several mN appear. The frequency and amplitude of the force peaks consistently grow as more particles are added into the interface, as seen in Figs. 1(c) and 1(d). The temporal fluctuations of the dissipation force are more intense for large particles ($\Delta = 1.45$) than for smaller ones ($\Delta = 0.5$) but are qualitatively similar for ordered and disordered surfaces. In general, the magnitude of the frictional force peaks is higher for larger Δ. This trend is consistent for all systems within the tested range. The emerging frictional resistance is directly attributable to third-body interactions since there is no measurable friction in a particle-free interface.

We quantify the frictional behavior of this system by extracting the shear force time-series (from the measured torque) for different N, number of particles and Δ, particle-to-asperity ratios. We calculate the average shear force, f_{ave}, by integrating the shear force time-series for a number of full rotations of the top plate and dividing by the corresponding duration. (Further details are included in the Supplemental Material [51].) This provides a quantitative measure of the system's frictional resistance.

The average frictional dissipation force, f_{ave}, increases monotonically with the number of particles and its magnitude strongly depends on the ratio of particle diameters

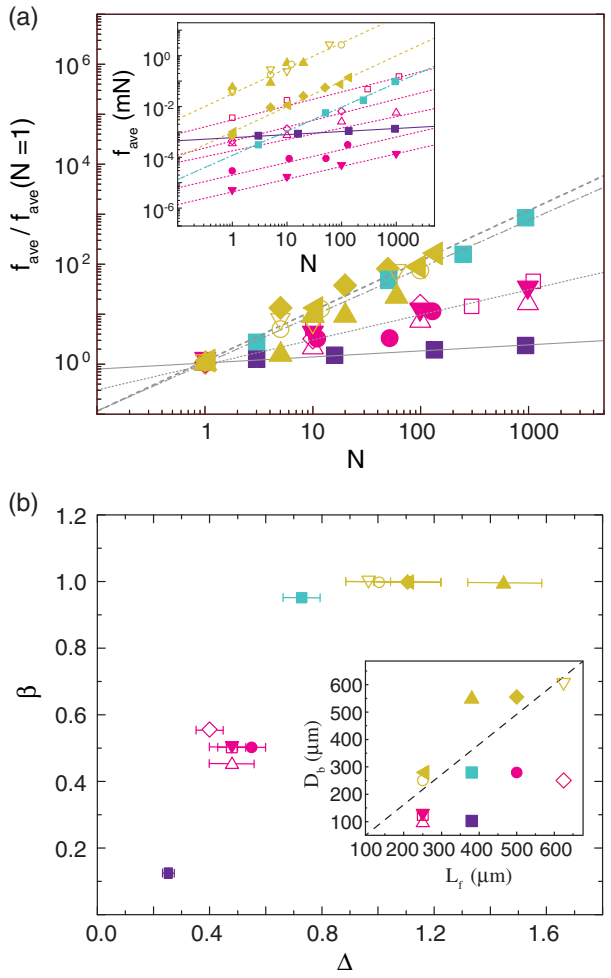

FIG. 2. Frictional resistance depends only on Δ and N. (a) The average shear force f_{ave} normalized by its single particle ($N = 1$) value as a function of the number of particles, N, for different $\Delta = D_b/L_f$. The inset shows the same data without normalization. The scaling $f_{\mathrm{ave}} \sim N^{\beta}$ is robust even though the proportionality factor may not be. The error bars represent the variation of particle size according to the manufacturer. (b) β as a function of Δ. ($\beta \sim 0.15$ for $\Delta = 0.26$, $\beta \sim 0.5$ for $\Delta = 0.5$, $\beta \sim 1.0$ for $\Delta = 1.45$). (inset) The marker symbols reveal the particle diameters D_b and asperity sizes L_f we used for the Δ's. Open (filled) symbols represent ordered (disordered) surfaces, respectively.

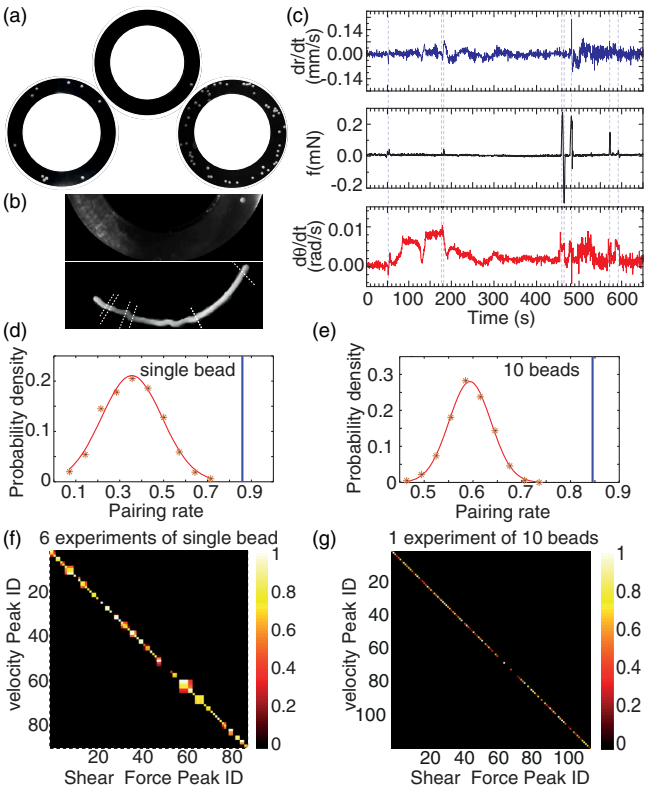

FIG. 3. Friction spikes correlate highly with discontinuities in the motion of third-body particles. (a) Three snapshots showing particles trapped between the two PDMS rings ($N = 1$, 10, 50 particles of size $D_b = 550$ μm on a disordered ring surface with $L_f = 500$ μm). (b) Composite image of a single-particle experiment showing the particle's entire trajectory. The dashed lines indicate where the force discontinuities occur. (c) Radial velocity (top), shear force (middle), and the angular velocity (bottom) of a single particle as a function of time. The dashed lines show where discontinuities of velocity and force occur. (d),(e) The success pairing rate of the cross-correlation of velocity spikes with shear force spikes as indicated by vertical blue lines is 0.8571 for single-particle experiments and 0.8475 for a 10-particle experiment. These success pairing rates are more than 3-sigma away from the Gaussian correlation (red curves) exhibited by synthetic data (stars). (f),(g) Cross-correlation matrix of velocity and shear force spikes for six single particle runs and for one 10-particle run.

and surface features [Fig. 2(a) and inset]. However, the slopes of the $f_{\mathrm{ave}} \sim N$ curves depend only on Δ, as shown in Fig. 2(a). Specifically, for $\Delta \geq 1$, the frictional force grows linearly with the number of trapped particles while for $\Delta \leq 1$, f_{ave} scales as N^{β} where $\beta \leq 1$ [Fig. 2(b)]. Interestingly, β does not depend on the surface pattern for a given Δ; it is the same for both ordered and disordered surfaces.

We image the interfacial dynamics while measuring the torque by affixing a 45° mirror between the bottom ring and the fixed plate of the rheometer, as shown in Figs. 1(a) and 3(a). Each friction event, which is reflected in the shear force signal as a force spike, is correlated with an abrupt particle displacement at the interface. We analyze the trajectories for each particle and compare them to the force time series. An interfacial image and the trajectory of a single particle over more than one full rotation is shown in Fig. 3(b). Particle velocities in the radial and azimuthal directions for a single particle experiment are plotted in Fig. 3(c). We note that most force spikes correspond to a sudden particle velocity change in the radial or azimuthal direction. We quantify the force-velocity spikes correlation using the phase difference $\exp(-|t_{\mathrm{vpeak}} - t_{\mathrm{fpeak}}|)$ where t_{vpeak} and t_{fpeak} are the times of occurrence of nearby

velocity and force spikes, respectively. The correlation rate is the ratio of the number of correlated pairs of friction and velocity spikes for several single-particle experiments [shown as colored blocks on the diagonal of Fig. 3(f)] over the total number of spikes. We compare our findings to the correlation of a random synthetic velocity time series containing the same number of spikes and the force signals of the corresponding time series. A success rate for 1000 null-hypothesis velocity profiles compared with the force time series follows a Gaussian distribution, as shown by the red curve in Fig. 3(d). The success rate for our single particle experiment, shown as the blue line in Fig. 3(d), is beyond a 3-sigma tolerance compared to the random artificial data. This indicates that the correlation between friction events and discontinuities in particle motion is significant for single-particle-induced friction. We extend this analysis to multiparticle friction by comparing the force signal with the trajectories of individual particles. The success pairing rate and phase difference shown in Figs. 3(e) and 3(g) further demonstrates the correlation between friction and particle motion for multiparticle experiments.

Discussion.—The top surface rotates at a constant rate, but the motion of the particles is intermittent, as shown in Fig. 3(c). This indicates that in addition to flowing along with the fluid (when $\Delta < 1$) or rolling between the surfaces (when $\Delta > 1$) particles occasionally jam between asperities of the two opposing surfaces. When a particle is trapped and released, it undergoes an abrupt velocity change in magnitude and/or direction. The discontinuous particle motion, induced by particle jamming and unjamming between asperities, highlights that the frictional force peaks appear when particles pin the interface during the shearing process and that, in our system, frictional dynamics are dominated by third-body interactions.

For $\Delta \geq 1$, many particles move erratically and change motion in a strongly inhomogeneous manner. For $\Delta < 1$, most particles have smoother trajectories with only a few particles showing sudden slope changes, as seen in two typical examples given in Figs. 4(a) and 4(b) and in Supplemental movies S1 and S2 [51]. Statistically, particles are generally slow moving and only occasionally experience higher speeds, as shown in the two examples of instantaneous velocity distributions in Figs. 4(c) and 4(d). The polyethylene third-body particles in our experiment are heavier than the silicone oil they are immersed in, and they settle to the stationary bottom surface. If both surfaces were completely flat, the steady rotation of the top plate would result in a spherical particle rolling on the bottom surface at a steady velocity dependent on its size, as indicated by the upward blue and red arrows in Fig. 4(e). The roughness of the surfaces distorts the shear flow, which advects in a tortuous path through a maze formed by the asperities. As a result, in our tests most particles move much slower than they would if the surfaces were flat.

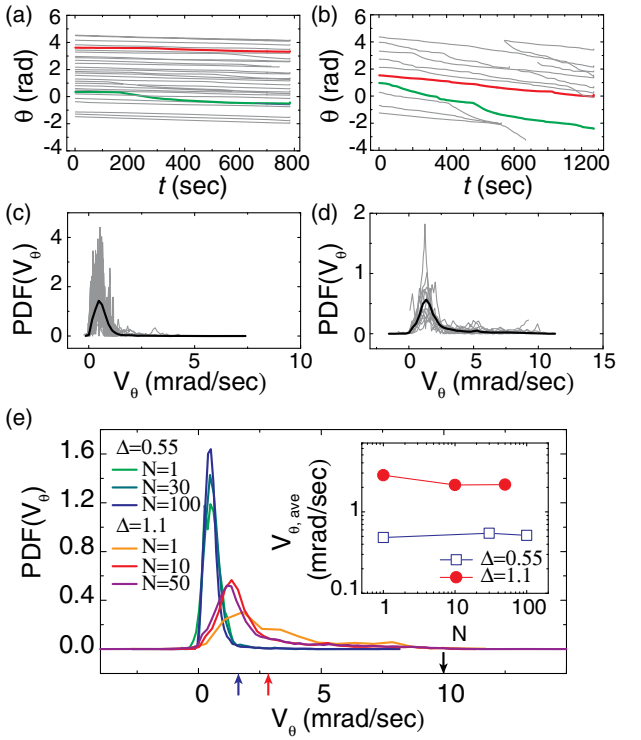

FIG. 4. Third-body particles' velocities statistics. (a),(b) Trajectories of individual particles unfolded in azimuthal angle $\theta(t)$ vs time for $\Delta = 0.55 < 1$ with $N = 30$ particles (left) and $\Delta = 1.1 \geq 1$ with $N = 10$ particles (right). We colored with red and green the trajectory of the particle that traveled the least and most distance out of all the particles that we successfully tracked in the entirety of the experiment. (c),(d) The respective distributions of instantaneous velocities of (a),(b). The thick line is the total distribution of all the particles instantaneous velocities. (e) The total particle instantaneous velocity distributions for $N = 1$, 30, 100 with $\Delta = 0.55$ and $N = 1$, 10, 50 with $\Delta = 1.1$. (inset) The average particle speed as a function of particle number N. The black downward arrow indicates the imposed rotational speed of the top plate; the blue and red upward arrow indicates the expected fluid speed at the center of a small ($\Delta = 0.55$) or large ($\Delta = 1.1$) particle for a linear laminar profile from the stationary bottom plate to the top steady moving plate (assuming no roughness present).

Occasionally, a particle may lift off the bottom plate and interact directly with the top rotating plate, or both plates, achieving significantly higher instantaneous speeds, indicated by the enhanced high-velocity tail of the distributions in Fig. 4(e). Individual particles may momentarily exceed the rotational speed of the top plate, indicated with a downward black arrow in Fig. 4(e). However, the average velocity does not depend significantly on the number of particles, as shown in inset to Fig. 4(e).

For smaller values of Δ, particles can hide better in the bottom surface's roughness and avoid getting pinned by opposing asperities, giving rise to a less erratic behavior both in their forces and their speeds. The bigger the particles are, the more often and more strongly they will

pin the two surfaces together and generate a force spike. The Δ-dependent scaling of frictional dissipation force with N and the presumably related Δ dependence of the velocity statistics remain open questions that may be resolved in the future by considering the way the particles interact with asperities and with each other.

This work was supported by the National Science Foundation through the Harvard Materials Research Science and Engineering Center (DMR-1420570). S. M. R. acknowledges support from the Alfred P. Sloan Foundation.

*Corresponding author.
shmuel@seas.harvard.edu
†These authors contributed equally to this work.

[1] F. P. Bowden, F. P. Bowden, and D. Tabor, *The Friction and Lubrication of Solids*, Vol. 1 (Oxford University Press, Oxford, 2001).
[2] B. N. J. Persson, *Sliding Friction: Physical Principles and Applications* (Springer-Verlag, Berlin, Heidelberg, 2013).
[3] T. Baumberger and C. Caroli, Solid friction from stick–slip down to pinning and aging, Adv. Phys. **55**, 279 (2006).
[4] J. H. Dieterich, Time-dependent friction and the mechanics of stick-slip, in *Rock Friction and Earthquake Prediction*, Contributions to Current Research in Geophysics (CCRG) (Birkhäuser, Basel, 1978), pp. 790–806.
[5] J. H. Dieterich, Modeling of rock friction: 1. Experimental results and constitutive equations, J. Geophys. Res. **84**, 2161 (1979).
[6] A. Ruina, Slip instability and state variable friction laws, J. Geophys. Res. **88**, 10359 (1983).
[7] S. M. Rubinstein, G. Cohen, and J. Fineberg, Visualizing stick–slip: Experimental observations of processes governing the nucleation of frictional sliding, J. Phys. D **42**, 214016 (2009).
[8] P. J. Blau, The significance and use of the friction coefficient, Tribol. Int. **34**, 585 (2001).
[9] S. M. Rubinstein, G. Cohen, and J. Fineberg, Detachment fronts and the onset of dynamic friction, Nature (London) **430**, 1005 (2004).
[10] I. Svetlizky and J. Fineberg, Classical shear cracks drive the onset of dry frictional motion, Nature (London) **509**, 205 (2014).
[11] S. M. Rubinstein, G. Cohen, and J. Fineberg, Dynamics of Precursors to Frictional Sliding, Phys. Rev. Lett. **98**, 226103 (2007).
[12] T. Yamaguchi, Y. Sawae, and S. M. Rubinstein, Effects of loading angles on stick–slip dynamics of soft sliders, Extreme Mech. Lett. **9**, 331 (2016).
[13] O. Ben-David and J. Fineberg, Static Friction Coefficient Is Not a Material Constant, Phys. Rev. Lett. **106**, 254301 (2011).
[14] O. Ben-David, S. M. Rubinstein, and J. Fineberg, Slip-stick and the evolution of frictional strength, Nature (London) **463**, 76 (2010).
[15] J. R. Rice and A. L. Ruina, Stability of steady frictional slipping, J. Appl. Mech. **50**, 343 (1983).
[16] S. M. Rubinstein, G. Cohen, and J. Fineberg, Contact Area Measurements Reveal Loading-History Dependence of Static Friction, Phys. Rev. Lett. **96**, 256103 (2006).
[17] P. Berthoud, T. Baumberger, C. G'Sell, and J.-M. Hiver, Physical analysis of the state- and rate-dependent friction law: Static friction, Phys. Rev. B **59**, 14313 (1999).
[18] C. Marone, Laboratory-derived friction laws and their application to seismic faulting, Annu. Rev. Earth Planet Sci. **26**, 643 (1998).
[19] C. Marone, The effect of loading rate on static friction and the rate of fault healing during the earthquake cycle, Nature (London) **391**, 69 (1998).
[20] S. Dillavou and S. M. Rubinstein, Nonmonotonic Aging and Memory in a Frictional Interface, Phys. Rev. Lett. **120**, 224101 (2018).
[21] M. Godet, The third-body approach: A mechanical view of wear, Wear **100**, 437 (1984).
[22] M. Godet, Third-bodies in tribology, Wear **136**, 29 (1990).
[23] Y. Berthier, Maurice Godet's third body, in *Tribology Series*, The Third Body Concept Interpretation of Tribological Phenomena Vol. 31, edited by D. Dowson, C. M. Taylor, T. H. C. Childs, G. Dalmaz, Y. Berthier, L. Flamand, J. M. Georges, and A. A. Lubrecht (Elsevier Science, Amsterdam, The Netherlands, 1996), pp. 21–30.
[24] K. Kato, Wear in relation to friction—A review, Wear **241**, 151 (2000).
[25] H. C. Meng and K. C. Ludema, Wear models and predictive equations: Their form and content, Wear 10th Int. Conf. Wear Mater., **181–183**, 443 (1995).
[26] Ph. Stempflé, G. Castelein, and M. Brendlé, Influence of environment on the size of the elemental wear debris of graphite, in *Tribology Series*, Boundary and Mixed Lubrication Vol. 40, edited by D. Dowson, M. Priest, G. Dalmaz, and A. A. Lubrecht (Elsevier Science, Amsterdam, The Netherlands, 2002), pp. 295–304.
[27] P. Stempflé and J. von Stebut, Nano-mechanical behaviour of the 3rd body generated in dry friction—Feedback effect of the 3rd body and influence of the surrounding environment on the tribology of graphite, Wear **260**, 601 (2006).
[28] J. Vande Voort and S. Bahadur, The growth and bonding of transfer film and the role of CuS and PTFE in the tribological behavior of PEEK, Wear 10th Int. Conf. Wear Mater. **181–183**, 212 (1995).
[29] S Fayeulle and I. L Singer, Friction behavior and debris formation of titanium-implanted 52100 steel, Mater. Sci. Eng. A, **115**, 285 (1989).
[30] Y. Berthier, M. Godet, and M. Brendle, Velocity accommodation in friction, Tribol. Trans. **32**, 490 (1989).
[31] M. C. Brendlé, P. H. Diss, and F. J. Spano, 3d optical-profilometric assessment of transfer and its significance for the mechanisms of primary particle detachment and wear, Wear **225–229**, 417 (1999).
[32] J. T. Uhl *et al.*, Universal quake statistics: From compressed nanocrystals to earthquakes, Sci. Rep. **5**, 16493 (2015).
[33] Y. Ben-Zion and C. G. Sammis, Characterization of fault zones, Pure Appl. Geophys. **160**, 677 (2003).
[34] C. G. Sammis and R. L. Biegel, Fractals, fault-gouge, and friction, Pure Appl. Geophys. **131**, 255 (1989).
[35] C. Sammis, G. King, and R. Biegel, The kinematics of gouge deformation, Pure Appl. Geophys. **125**, 777 (1987).

[36] C. Marone and C. H. Scholz, Particle-size distribution and microstructures within simulated fault gouge, J. Struct. Geol. Frict. Phenom. Rock **11**, 799 (1989).
[37] X. Chen, A. S. Elwood Madden, and Z. Reches, Powder rolling as a mechanism of dynamic fault weakening, in *Fault Zone Dynamic Processes* (American Geophysical Union (AGU), Washington, D.C., 2017), pp. 133–150.
[38] A. Sagy, E. E. Brodsky, and G. J. Axen, Evolution of fault-surface roughness with slip, Geology **35**, 283 (2007).
[39] E. E. Brodsky, J. D. Kirkpatrick, and T. Candela, Constraints from fault roughness on the scale-dependent strength of rocks, Geology **44**, 19 (2016).
[40] J.-C. Géminard, W. Losert, and J. P. Gollub, Frictional mechanics of wet granular material, Phys. Rev. E **59**, 5881 (1999).
[41] W. Losert, J.-C. Géminard, S. Nasuno, and J. P. Gollub, Mechanisms for slow strengthening in granular materials, Phys. Rev. E **61**, 4060 (2000).
[42] T. Divoux and J.-C. Géminard, Friction and Dilatancy in Immersed Granular Matter, Phys. Rev. Lett. **99**, 258301 (2007).
[43] G. D. R. MiDi, On dense granular flows, Eur. Phys. J. E **14**, 341 (2004).
[44] P. Jop, Y. Forterre, and O. Pouliquen, A constitutive law for dense granular flows, Nature (London) **441**, 727 (2006).
[45] Y. Forterre and O. Pouliquen, Flows of dense granular media, Annu. Rev. Fluid Mech. **40**, 1 (2008).
[46] M. H. Müser, L. Wenning, and M. O. Robbins, Simple Microscopic Theory of Amontons's Laws for Static Friction, Phys. Rev. Lett. **86**, 1295 (2001).
[47] R. Aghababaei, D. H. Warner, and J.-F. Molinari, On the debris-level origins of adhesive wear, Proc. Natl. Acad. Sci. U.S.A. **114**, 7935 (2017).
[48] M. H. Müser, M. Urbakh, and M. O. Robbins, Statistical mechanics of static and low-velocity kinetic friction, in *Advances in Chemical Physics* (Wiley-Blackwell, New York, NY, 2003), pp. 187–272.
[49] M. Cieplak, E. D. Smith, and M. O. Robbins, Molecular origins of friction: The force on adsorbed layers, Science **265**, 1209 (1994).
[50] P. A. Thompson and M. O. Robbins, Origin of stick-slip motion in boundary lubrication, Science **250**, 792 (1990).
[51] See Supplemental Material at http://link.aps.org/supplemental/10.1103/PhysRevLett.122.135503 for experimental videos and details, and explanations of the average force calculation, and the correlation method of force spikes with particle velocity spikes.